

# A Wideband Reflectarray Based on Single-Layer Magneto-Electric Dipole Elements with 1-Bit Switching Mode

Wen Wu, Kai-Da Xu, *IEEE Senior Member*, Qiang Chen, *IEEE Senior Member*, Toru Tanaka, Masaki Kozai, and Hiroya Minami

**Abstract**—A single-layer wideband low-cost linearly polarized reflectarray with 1-bit magneto-electric (ME) dipole as the unit cell is presented. The  $180^\circ$  reflection phase difference between the two states for the unit cell is realized by switching the ground-signal-ground transmission line between “open” and “short” to the ground in the ME dipole structure. The corresponding numerical simulations of the reflectarray unit cell show that the bandwidth of the reflection phase difference within  $180^\circ \pm 20^\circ$  is more than 34% under both normal and oblique incidences. Moreover, the insertion loss is lower than 0.35 dB over the entire Ku-band benefiting from the concise phase shifting structure. Two static reflectarray prototypes for collimated beam at  $\theta = 15^\circ$ ,  $\varphi = 0^\circ$  and  $\theta = 15^\circ$ ,  $\varphi = 90^\circ$  are designed and fabricated. The measurement results of the reflectarray verify a great advantage of wideband performance, with over 32% bandwidth for 1.5-dB gain variation below the maximum value in both  $\varphi = 0^\circ$  and  $\varphi = 90^\circ$  planes.

**Index Terms**—Magneto-electric (ME) dipole, reflectarray, wideband antenna, low cost, periodic structures.

## I. INTRODUCTION

The demands for data centers are accelerating due to global digital transformation. Hence, container-type data centers that can be built flexibly are attracting attention [1][2]. However, the effects of signal fading caused by electromagnetic scattering by buildings and other shielding is always a challenge in connecting container-type data centers to high-speed, wideband, low-latency 5G/beyond 5G (B5G) radio access networks (RANs). Intelligent reflect surface (IRS) was introduced to address this issue. As a common form of IRS, the reflectarray attracts a great deal of research, due to its attractions in the planar structure, low profile, light weight, and flexibility of fabrication [3]-[5]. The collimated beam can be realized by controlling reflection phase of each unit cell in the reflectarray [6]. Therefore, the aperture can be considered to be filled with many discrete spatial phase shifters. Phase quantization is introduced to assign the reflection phase of the reflectarray unit cell. The most easily implemented phase quantization is 1 bit switching scheme, which separates the continuous  $360^\circ$  phase range into only two discrete values of  $0^\circ$  and  $180^\circ$ . It was reported in [7] [8] that compared to the precise phase distribution reflectarray, phase errors caused by 1-bit phase quantization may lead to performance degradation such as lower gain and higher side lobe level (SLL). Nevertheless, owing to the huge advantages in cost and

This work was supported in part by the Program on Open Innovation Platform with Enterprises, Research Institute and Academia, Japan Science and Technology Agency (JST, OPERA, JPMJOP1852). (Corresponding author: Kai-Da Xu.)

W. Wu and Q. Chen are with the Department of Communications Engineering, Tohoku University, Sendai 980-8579, Japan.

K. D. Xu is with the School of Information and Communications Engineering, Xi'an Jiaotong University, Xi'an 710049, China. (e-mail: kaidaxu@ieee.org)

T. Tanaka, M. Kozai and H. Minami are with the NTT Space Environment and Energy Laboratories, NTT Corporation, Tokyo 180-8585, Japan.

complexity, 1-bit phase quantization has been widely used for reflectarrays.

However, it has been shown in several studies that reflectarrays suffer from narrow bandwidth performance, which is primarily caused by two factors [9]-[12]: 1) the differences in spatial phase delays caused by different electrical path lengths from the feed to each unit cell and 2) the inherent narrow bandwidth resonance characteristics of reradiation element in the unit cell.

For the reflectarray based on 1-bit reconfigurable unit cell, the bandwidth suffers from further compression due to the additional phase quantization error. In [13], the unit cell achieves reflection phase reversal by switching between equivalent electric and magnetic walls, and the bandwidth of  $180^\circ$  phase difference can reach 60%, but the 1.5-dB gain bandwidth of the reflectarray shrinks to 21% due to the inherent narrowband reradiation characteristics of the electric dipole. The polarization-rotating unit cell in [14] achieved ultra-wideband for  $180^\circ$  phase difference, but was also limited by the narrowband reradiation characteristics, where the 3 dB bandwidth of the reflectarray is reduced to 18.7%.

Therefore, the critical issue of solving the bandwidth problem is to implement a frequency-independent design for both of radiating and phase-shifting elements in the unit cell. Considering this, a magneto-electric (ME) dipole with proper feeding is a good candidate for the design of reflectarray unit cell, benefiting from the frequency independent characteristics brought by the complementary structure. However, very few designs of reconfigurable reflectarrays using ME dipoles have been reported so far. In [15], the ME dipole was deployed in reflectarray antenna, but reconfigurable feature was not available due to the use of element rotation method.

This communication is organized as follows. Section II presents the working principle and performance of the 1-bit ME dipole element. The design procedure for the broadband reflectarray is described in Section III, while the simulated and measured results of the  $16 \times 16$  static prototypes are analyzed and discussed. Finally, Section IV concludes the article.

## II. 1-BIT REFLECTARRAY UNIT CELL BASED ON ME DIPOLE

ME dipole is a complementary structure through combining an electric dipole with a magnetic dipole formed by the open end of a vertically-located patch antenna [16][17]. If the magnetic dipole and electric dipole resonate at the same frequency, the imaginary part of the input impedance of the ME dipole antenna can be eliminated. Moreover, the electric dipole and the magnetic dipole should be excited with equal power and equal phase. By this way, the ME dipole can achieve stable gain, pattern, beam width, input impedance and other performance over wide frequency range.

### A. Structure of the 1-Bit Reflectarray Unit Cell

In [18], the ME dipole was originally proposed as a single radiating antenna. The feed design is still difficult and thus has not been used in conventional array antenna so far, however for space-fed reflectarrays,

the complexities in feed design can be simplified by introducing ingenious 1-bit switching structure to the feed point. As a result, the wideband performance and the 1-bit switching function can be achieved simultaneously. Based on this idea, a new 1-bit wideband reflectarray unit cell is proposed.

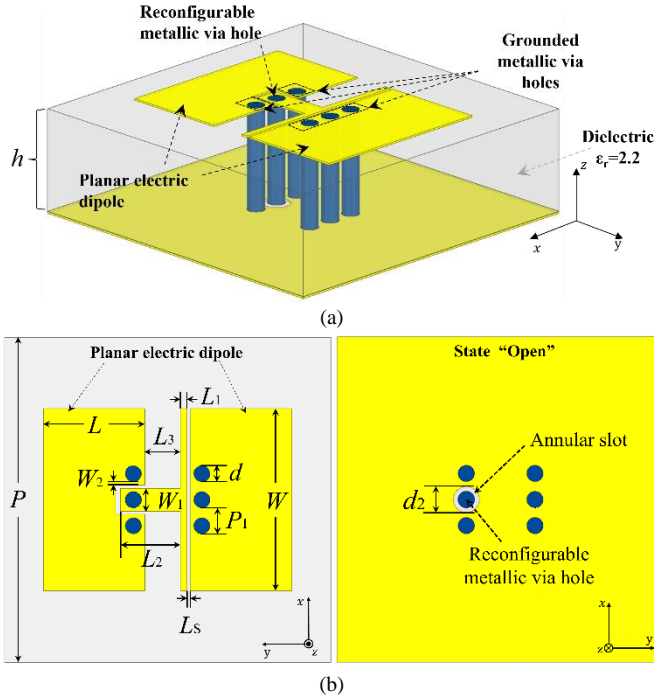


Fig. 1. (a) 3-D topology of the proposed wideband ME dipole unit cell with state 0. (b) Top surface and bottom ground of the unit cell with state “open” (i.e., state 0). Yellow represents metal, gray represents dielectric substrates, and dark blue represents metallic via holes.

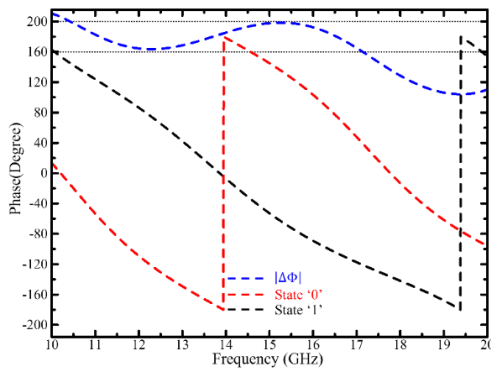


Fig. 2. Phase of reflection coefficient of 1-bit reflectarray unit cell with  $W=5.6$  mm,  $L=3.6$  mm under normal incidence.

A planar electric dipole is coated on the dielectric substrate with a thickness  $h$  of 3.0 mm and a relative dielectric constant of 2.2, as shown in Fig. 1(a). The arm length of the electric dipole is  $L$  and the width is  $W$ , as shown in Fig. 1(b). The magnetic dipole consists of two vertical electric walls, which are formed by two rows of metallic via holes with a quarter-wavelength height located on the inner edge of each half planar electric dipole. A via hole in the middle of the row is connected to a T-shaped coupled strip as the reconfigurable metallic via hole, while the other five via holes are directly shorted to the ground. Based on this structure, the ground-signal-ground (GSG) transmission line can be constructed by the reconfigurable via hole in the middle and two grounded via holes on two sides. The annular slot on the bottom metallic layer encircling the reconfigurable metallic via hole enables the ideal switching function between “open” and “short” to the ground.

Initially, the ME dipole is used for transceiver antenna and the impedance of the GSG transmission line should be matched with the feeding network. However, in the space-fed reflectarray unit cell, the ME dipole will be operated as a scatterer and there is no need to consider the matching of the resonant unit cell with the feeding network. If the “open” and “short” switching is operated at the bottom annular slot of the GSG transmission line as shown in Fig. 1(b), the reflection phase will be reversed from  $0^\circ$  to  $180^\circ$  which is denoted as state 0 and state 1 in 1-bit phase quantization. The  $180^\circ$  phase difference will be stable at a wide frequency range because of the frequency independent characteristics from the classic transmission line theory, as equation (1) shown below.

$$\Gamma = \frac{Z_L - Z_0}{Z_L + Z_0} \quad (1)$$

where  $Z_0$  is the characteristic impedance of the GSG transmission line. When the load impedance  $Z_L$  is infinite or 0, the reflection coefficient  $\Gamma$  will be 1 or -1, which provides the frequency independent reflection phase  $0^\circ$  and  $180^\circ$ , respectively. Therefore, if the “open” and “short”

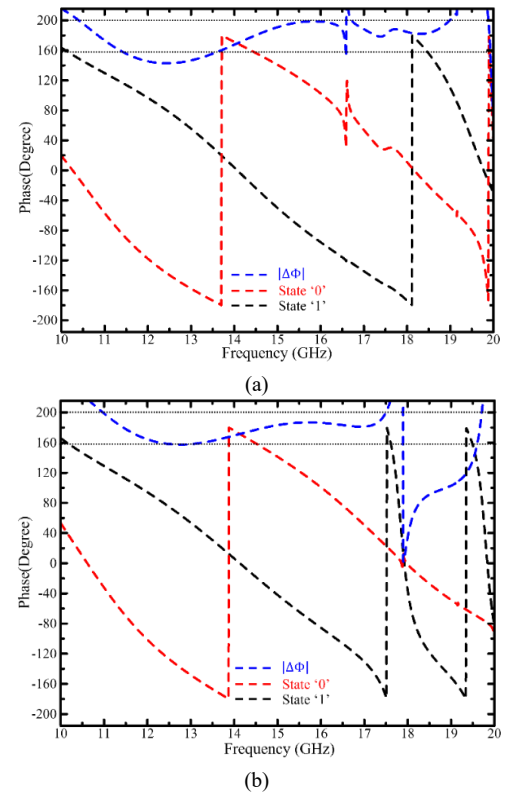


Fig. 3. Simulated phase of reflection coefficient under oblique incidence with  $\theta=25^\circ$  for (a) TE mode and (b) TM mode.

operation states are implemented to the end of GSG transmission line, the  $180^\circ$  phase difference can be obtained with a very wide bandwidth.

The geometry parameters including the electric dipole armlength ( $L$ ), the width of ME dipole ( $W$ ), the via hole spacing ( $P_1$ ) and unit cell period ( $P$ ) are evaluated to obtain the proper resonance frequency and bandwidth. Ansys HFSS electromagnetic solver is used to perform numerical simulations for the single unit cell with Periodic boundaries and Floquet port excitations. For normal incidence, the simulated reflection coefficient of the ME dipole reflectarray unit cell is shown in Fig. 2.  $|\Delta\Phi|$  represents the reflection phase difference between state 0 and state 1, which has a value of  $180^\circ \pm 20^\circ$  from 10.5 GHz to 17.5 GHz with a bandwidth of 38%. In reflectarray, however, the reflection coefficient of the unit cell under oblique incidence is compulsory to be investigated to ensure the performance of the edge region of the

reflectarray.

### B. Performance under Oblique Incidence

The oblique incidence can be decomposed into two orthogonal modes: TE mode and TM mode. According to the typical configuration of the focal-to-diameter ( $f/D$ ) ratio around 1.07 [11], the oblique incidence angle  $\theta$  should be investigated with  $25^\circ$  as the maximum. For the case of TE mode, the effective length of magnetic dipole constructed by vertically-located patch antenna will be shrunk as the value of elevation angle  $\theta$  increases. Similarly, for the case of TM mode, the effective arm length of the electric dipole will be shrunk as the angle  $\theta$  increases. If the difference between resonant frequencies of the magnetic dipole and the electric dipole is excessive, the ME dipole's complementary feature will be destroyed and the reflection phase of the reflectarray unit cell will be observed to be strongly nonlinear in the operating band, resulting in the unstable  $180^\circ$  phase difference. Consequently, the bandwidth of the  $180^\circ \pm 20^\circ$  reflection phase difference will be severely worsened.

It should be noted that the resonance performance of the magnetic dipole in the proposed ME dipole unit cell is very sensitive to the width of the patch antenna  $W$ , while changing the electric dipole length  $L$  has a relatively small effect on the resonant performance of the electric dipole. As a result, the TE mode will introduce serious resonant mismatch between magnetic dipole and electric dipole, leading to the variation of  $180^\circ$  reflection phase difference. The simulation results show that when the incidence angle is  $\theta=25^\circ$ , the reflection phase difference is lower than  $160^\circ$  from 11.4 GHz to 13.7 GHz and an abrupt change exists at around 16.6 GHz, as shown in Fig. 3(a). In contrast, the TM mode maintains a stable reflection phase difference with bandwidth of 32%, as shown in Fig. 3(b), which is almost same as that under normal incidence.

TABLE I  
DIMENSIONAL DETAILS OF THE REFLECTARRAY UNIT CELL

Parameter	$P$	$P_1$	$d$	$d_2$	$L$	$W$
Value (mm)	10	0.8	0.5	0.8	3.1	5.0
Parameter	$W_1$	$W_2$	$L_1$	$L_2$	$L_3$	$L_s$
Value (mm)	0.7	0.15	0.2	1.85	0.8	0.1

As indicated, the improvement will be concentrated on resolving the bandwidth shrink at TE mode. An efficient way is to reduce the dimensions of the magnetic dipole. The values of  $L$  and  $W$  can be chosen through tuning the reflection phase difference. On the other hand, with the fixed thickness of substrate, if these two values are decreased significantly, severe mismatch will be observed between the electric and magnetic dipoles, leading to the failure of the complementary characteristics of the ME dipole and a dramatic reduction in bandwidth. Therefore, the values of  $L$  and  $W$  are reduced to  $3.1$  mm and  $5.0$  mm, respectively, and the unit cell spacing is set to be  $0.47 \lambda_0$ , where  $\lambda_0$  is the wavelength at the center frequency of 14 GHz, to avoid grating lobe. The simulated reflection phase difference is maintained at  $180^\circ \pm 20^\circ$  from 12.6 GHz to 17.8 GHz with a bandwidth of 34% for the oblique incidence angle  $\theta$  from  $0^\circ$  to  $25^\circ$  and the insertion loss is less than 0.35 dB over the entire  $Ku$ -band. The detailed geometry of the reflectarray unit cell is tabulated in Table I.

Considering that the proposed unit cell will be deployed for the future dynamic reconfigurable reflectarray, the performance of reconfigurable ME dipole with PIN diode is investigated. The commercial PIN diode MA4AGFCP910 is selected to achieve the operations of "open" and "short" for the reconfigurable metallic via hole with low insertion loss and high isolation. The PIN diode model has been well established and validated in application [7]. The state

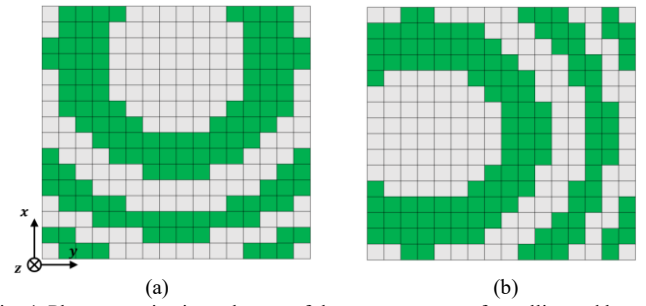


Fig. 4. Phase quantization schemes of the two prototypes for collimated beams of (a)  $\theta=15^\circ$ ,  $\varphi=0^\circ$ , and (b)  $\theta=15^\circ$ ,  $\varphi=90^\circ$ . Green block represents the unit cell with state 0 and gray block represents the unit cell with state 1.

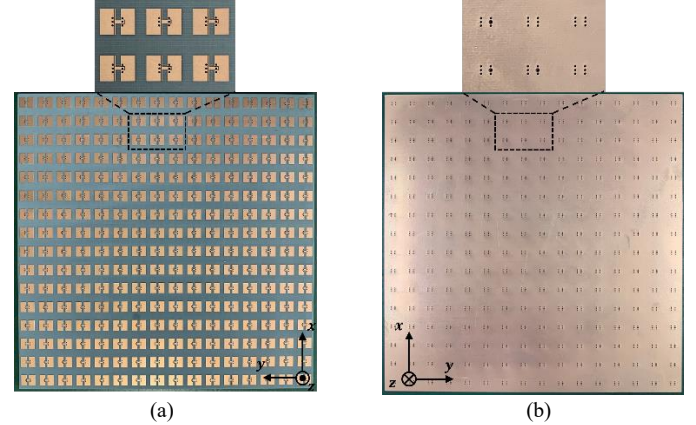


Fig. 5. Photograph of the reflectarray prototype (a) top view, (b) bottom view.

"on" is modeled as a lumped resistance ( $R$ ) of 5 Ohm connected in series with an inductance ( $L$ ) of 30 pH and the state "off" is modeled as a lumped capacitance ( $C$ ) of 35 fF connected in series with inductance ( $L$ ) of 30 pH. The performance of the unit cell based on PIN diode is simulated. The result shows that the bandwidth of  $180^\circ \pm 20^\circ$  reflection phase difference moves toward low frequency with the change of about 1 GHz and the insertion loss increases to a maximum of 1.34 dB due to the insertion of PIN diode.

### III. PROTOTYPE DESIGN AND CHARACTERIZATION

To validate the wideband performance, the proposed reflectarray is deployed using  $16 \times 16$  unit cells with an overall size of  $160 \times 160$  mm<sup>2</sup>. The reflectarray is illuminated by a  $Ku$ -band linear polarization standard gain horn antenna, whose power pattern can be approximated by  $\cos^{2q}(\theta)$  model with the  $q$  value of 24. The value of  $f/D$  is selected as 1.07 to guarantee that the illumination power at the edge of the aperture is below -12 dB for the central feed case, which implies the horn antenna is located above the center of the reflectarray.

Two prototypes are designed for two collimated beam directions:  $\theta=15^\circ$ ,  $\varphi=0^\circ$  and  $\theta=15^\circ$ ,  $\varphi=90^\circ$ . The required precise phase compensation  $\psi_{mn}$  of the unit cell in  $m$ th column and the  $n$ th row ( $m, n = 1, 2, \dots$ ) can be calculated as

$$\psi_{mn} = k_0 d_{mn} + \varphi_{mn} + \Delta\varphi \quad (2)$$

where  $k_0$  is the free space wavenumber,  $\varphi_{mn}$  is the progressive phase (pp) of the  $(m, n)$ th unit cell for collimated beam in the specific direction,  $d_{mn}$  is the distance from the phase center of the feed to the  $(m,n)$ th unit cell.  $\Delta\varphi$  is added to provide an additional degree of freedom for the reflectarray design, which can be selected in the range from 0 to  $2\pi$ . The phase quantization error can be optimized by the value of  $\Delta\varphi$  [19] to achieve a flat gain response over wide frequency band. For  $Ku$ -band, the value of  $k_0$  is calculated at 14 GHz. The

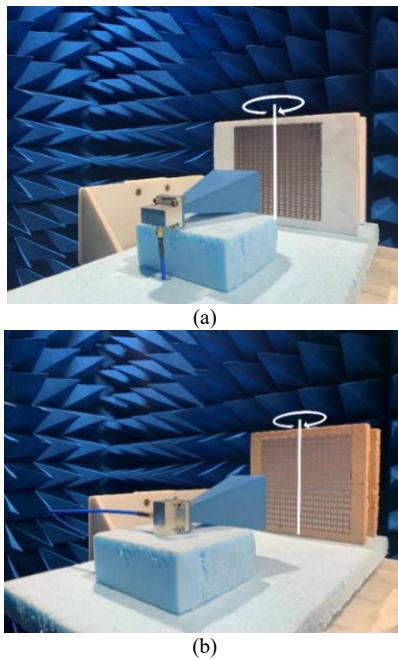


Fig. 6. Measurement setup for (a) prototype with collimated beam:  $\theta = 15^\circ$ ,  $\phi = 0^\circ$  and (b) prototype with collimated beam:  $\theta = 15^\circ$ ,  $\phi = 90^\circ$ .

maximum phase error caused by frequency dispersion can be evaluated by [11]:

$$\text{phase error} = (k - k_0)(\sqrt{f^2 + D^2/4} - f) \quad (3)$$

where  $f$  is the height of feed above the center of the reflectarray surface,  $D$  is the diameter of the aperture. At the frequencies of 13 GHz and 18

GHz, the phase errors at the edge of the reflectarray will be  $20^\circ$  and  $80^\circ$ , respectively. Therefore, the impact of gain will be less than 0.1 dB and 0.5 dB, respectively, due to the illumination power tapering. Considering the fact that the gain of the reflectarray is usually enhanced as the frequency increases for the same physical dimension, consequently, the flatness of the gain will be improved.

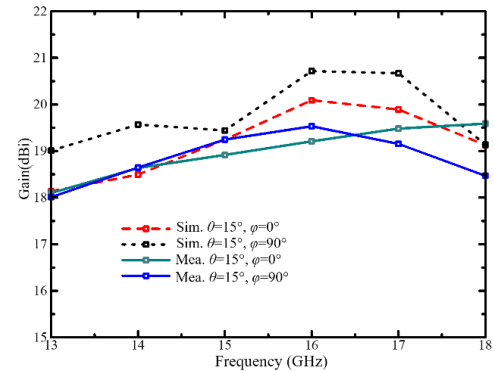


Fig. 7. Comparisons of measured and simulated reflectarray gains.

Since the feed is approximated as a point source, the phase center of the horn antenna needs to be evaluated by numerical simulation for the far-field radiation phase distribution using electromagnetic simulator ANSYS HFSS. The phase center will be a little different, when the frequency varies. Accordingly, the value of  $f/D$  is 1.09 and 1.15 at the frequencies 13 GHz and 18 GHz, respectively.

The 1-bit phase quantification of the  $(m, n)$ th unit cell can be obtained by:

$$\text{State} = \begin{cases} 0, & 0 \leq \text{mod}(\psi_{mn}, 2\pi) < \pi \\ 1, & \pi \leq \text{mod}(\psi_{mn}, 2\pi) < 2\pi \end{cases} \quad (4)$$

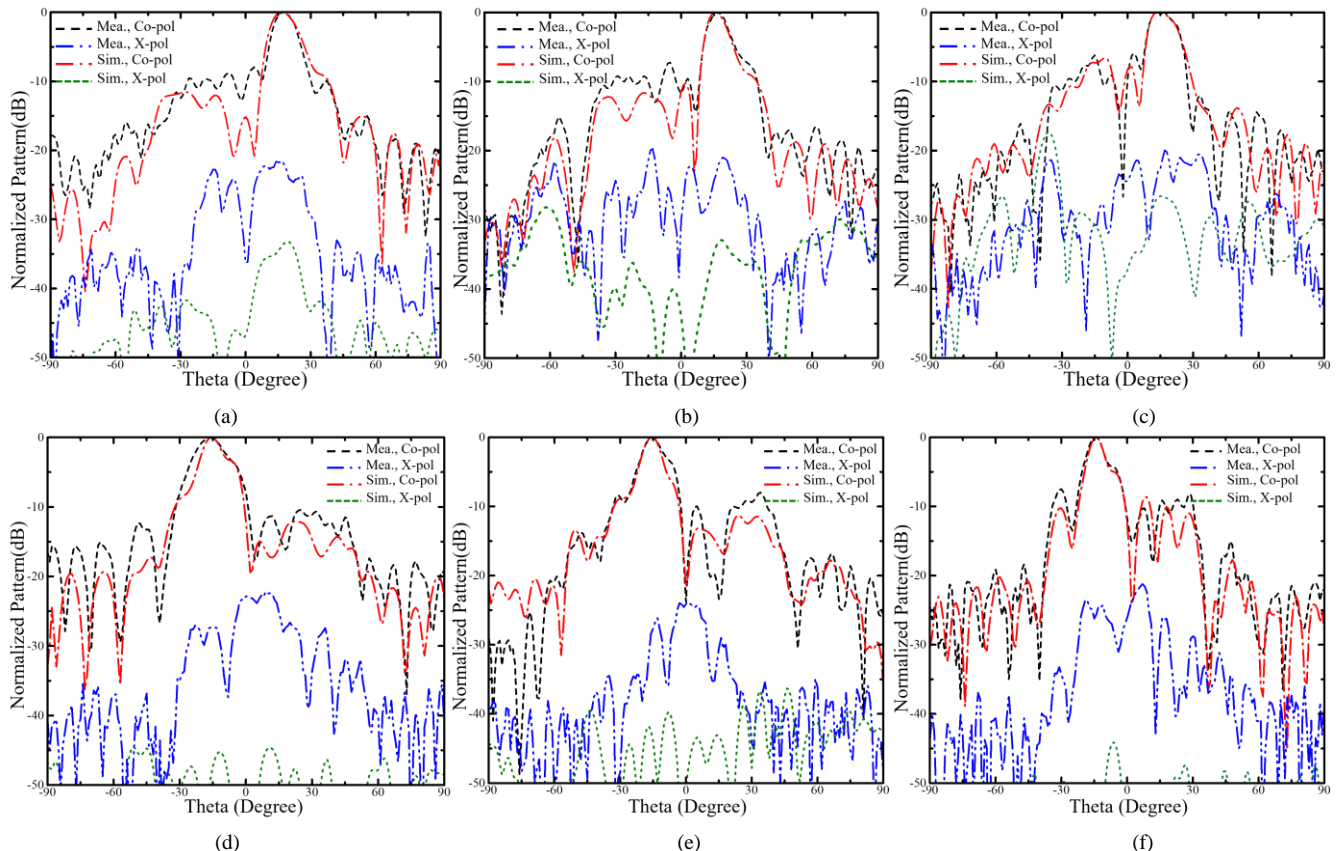


Fig. 8. Comparison of measured and simulated patterns. Scanning in  $\phi = 0^\circ$  plane at (a) 13.0, (b) 16.0, and (c) 18.0 GHz. Scanning in  $\phi = 90^\circ$  plane at (d) 13.0, (e) 16.0, and (f) 18.0 GHz.

TABLE II  
GAIN LOSS BUDGET FOR THE COLLIMATED BEAM

Factor	Loss (dB) at 13 GHz	Loss (dB) at 16 GHz	Loss (dB) at 18 GHz
Spillover	0.1	0.1	0.1
Illumination	1.9	2	1.7
1-bit quantization	2.9	3.1	3.5
Aperture Blockage	1.2	1.4	1.6
Element loss	0.1	0.1	0.2
Beam Scan	0.4	0.5	0.5
Specular reflection	1.95	2.2	2.4
Total	8.55	9.4	10.0

where  $\text{mod}(\psi_{mn}, 2\pi)$  is the modulo operation for the required precise phase compensation divided by  $2\pi$ . The reflection phase quantification states distributions of all unit cells can be mapped for collimated beam in these two reflectarray prototypes, as shown in Fig. 4. The fabricated static reflectarray prototype with collimated beam direction:  $\theta=15^\circ$ ,  $\varphi=90^\circ$  is shown in Fig. 5 with the zoom-in views for the top and bottom layers. All unit cells on the top metallic layer are the same while the annular slots on the bottom metallic layer are deployed for unit cells of state 0.

These two *Ku*-band wideband reflectarray prototypes are measured by rotating  $\theta$  angle from  $-90^\circ$  to  $90^\circ$  in the  $\varphi=0^\circ$  plane Measurement Results and discussion (i.e., *xoz*-plane) and  $\varphi=90^\circ$  plane (i.e., *yo**z*-plane), respectively, in the anechoic chamber, as shown in Fig. 6. The far-field performance in the scanning plane is recorded, then the gains and patterns are compared with the simulation ones, as shown in Figs. 7 and 8. Limited by bandwidth of the standard gain horn antenna, the

TABLE III  
COMPARISONS OF THE PROPOSED WIDEBAND REFLECTARRAY WITH OTHER REPORTED WORKS

Ref	Number of elements	Gain Bandwidth (%)	Reconfigurability
[12]	$35 \times 35$ ( $17\lambda \times 17\lambda$ )	16.7% (1.5-dB)	No
[13]	872 (Diameter: $14.4\lambda$ )	20.6% (1.5-dB) 28.6% ((2.0-dB)	Static
[14]	$50 \times 50$ ( $10\lambda \times 10\lambda$ )	40% (3.6-dB)	Static
[15]	$16 \times 16$ ( $5.8\lambda \times 5.8\lambda$ )	40% (5-dB)	No
[21]	$16 \times 16$ ( $7.1\lambda \times 7.4\lambda$ )	19% (2.0-dB)	Dynamic
[22]	$16 \times 16$ ( $8\lambda \times 8\lambda$ )	15.4% ((1.0-dB)	Dynamic
[23]	$12 \times 12$ ( $6.6\lambda \times 6.6\lambda$ )	8.4% (1.0-dB)	Dynamic
This work	$16 \times 16$ ( $8\lambda \times 8\lambda$ )	25% (1.0-dB) 32% (1.5-dB)	Static

frequency range is measured from 13 GHz to 18 GHz. The collimated beam in both  $\varphi=0^\circ$  plane and  $\varphi=90^\circ$  plane are realized in entire *Ku*-band as expected and the shape of the main lobes are well predicted. The measured cross-polarizations are all lower than -22 dB, showing high level of polarization isolation. The variation of gains is less than 1.5 dB within the entire *Ku*-band whose bandwidth is greater than 32% and the beam point error is lower than  $2^\circ$  within this bandwidth. The measured overall aperture efficiency is about 11% at center frequency.

Table II tabulates factors in the loss budget for the collimated beam of  $\theta=15^\circ$ ,  $\varphi=90^\circ$ . It shows that the efficiency loss is mainly caused by

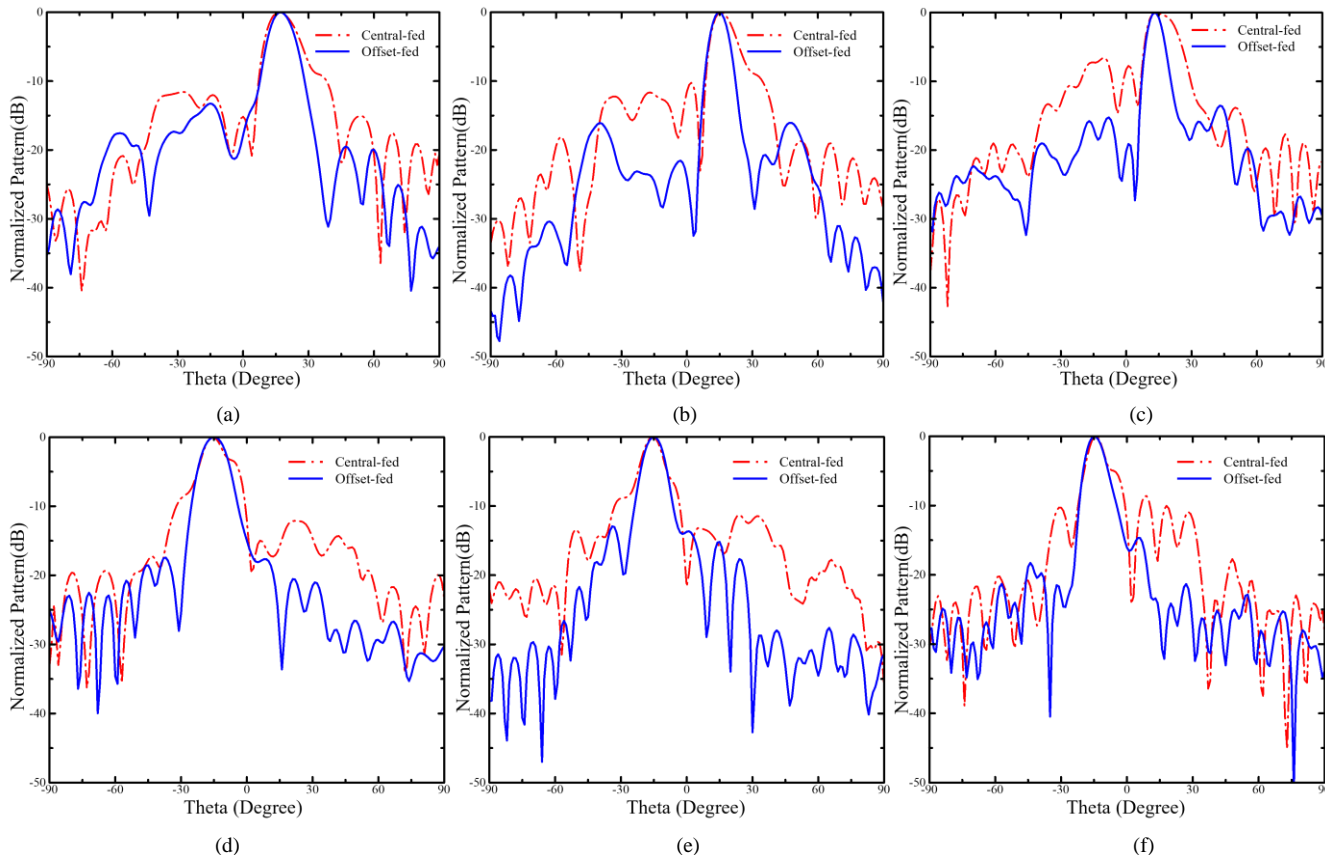


Fig. 9. Comparison of central-fed and offset-fed patterns. Scanning in  $\phi = 0^\circ$  plane at (a) 13.0, (b) 16.0, and (c) 18.0 GHz. Scanning in  $\phi = 90^\circ$  plane at (d) 13.0, (e) 16.0, and (f) 18.0 GHz.

illumination, feed blockage and specular reflection. Being fed by a standard gain (20 dBi) horn antenna, the loss due to illumination taper is up to 2 dB at 16 GHz as the edge taper of the reflectarray aperture is -12 dB. The aperture blockage effect also leads to gain loss, more importantly, it primarily results in high SLLs.

The deployed standard gain horn antenna has a very large volume and high directivity with an aperture size of  $3.6\lambda \times 2.7\lambda$  and flare length of  $6.4\lambda$  at 14 GHz. The phase center is located at 50 mm ~ 60 mm below the surface of the horn aperture within *Ku*-band, which means that for the central fed configuration in this work, there is only a distance of 0.8D between the surface of the horn aperture and the reflectarray aperture. The blockage ratio is commonly used to evaluate the aperture blockage effect and is defined as the ratio of the blockage diameter ( $D_B$ ) to the diameter of the reflectarray aperture  $D$  [5] [20]. The blockage diameter  $D_B$  is not the fixed physical diameter of horn antenna. Actually, it is an effective diameter which is dependent on the physical volume, collimated beam angle and operating frequency. Therefore, the aperture blockage effect varies with frequency, the gain loss caused by blockage is up to 1.6 dB at 18 GHz as listed in table II and corresponding SLLs are up to -7 dB, as observed in Fig. 8. In contrast, the blockage loss and degradation in beam pattern is comparatively lower at 13 GHz.

As indicated above, the critical aspect of improving the patterns of the proposed reflectarray is to reduce the blockage effect. To demonstrate this, we further investigated the offset-fed configuration for the reflectarray to relieve blockage effect of the feed. The offset angle is assigned as  $15^\circ$  in *yo**z*-plane, which means the angle from phase center of the feed horn antenna to the reflectarray aperture center is set as  $\theta=15^\circ$  at  $\varphi=90^\circ$ . With this offset feed, the SLLs are reduced by about 6 dB on average for both collimated beams over the entire *Ku* band with better beam pattern, as shown in Fig. 9.

Table III compares the proposed 1-bit static reflectarray with reported 1-bit wideband reflectarray. By introducing wideband radiation and frequency-independent phase shift structure in the design of the unit cell, stable gain and reflection phase difference are realized. Consequently, the proposed reflectarray has a great advantage in terms of gain bandwidth and is realized in single-layer structure at a low cost.

#### IV. CONCLUSION

A wideband reflectarray for the enhancement of gain bandwidth based on the linear polarization ME dipole elements has been proposed which maintains a stable reflection phase difference between the state 0 and state 1 over 34% bandwidth with extremely low power loss of -0.35 dB over the entire *Ku*-band. Consequently, the reflectarray based on the proposed unit cells achieves remarkable performance of gain bandwidth. Two reflectarray prototypes are fabricated for static beam collimation along two different directions to validate the gain stability within the operating band. It will be attractive due to the achievement of dynamic beamsweeping with electrically reconfiguration in unit cell, if some commercial electric switch devices (e.g., single-pole single-throw (SPST) switch, micro-electromechanical systems (MEMS)) are employed in our proposed design. Possibly, the gain bandwidth of the dynamic reconfigurable version would shrink compared to the proposed ideal static prototype using fixed passive switches [24] [25].

#### REFERENCES

[1] T. Otsuji, K. Iwatsuki, H. Yamada and M. Yashima, "Concept of resilient electric power and information communication technology (R-EICT) converged network systems based on overall optimization of autonomous decentralized cooperative control of DC microgrids," *2021 IEEE Power & Energy Society Innovative Smart Grid Technologies Conference (ISGT)*, 2021, pp. 1-5.

[2] T. Tanaka, H. Minami, et al. "Energy-distribution platform technologies toward zero environmental impact" *NTT Technical Review* Vol. 19 No. 6 June 2021

[3] J. Huang, "Microstrip reflectarray," *Proc. Antennas Propag. Soc. Int. Symp. Dig.*, Jun. 1991, vol. 2, pp. 612-615.

[4] J. Huang and J. A. Encinar, *Reflectarray Antennas*. Hoboken-Piscataway, NJ, USA: Wiley—IEEE Press, 2007.

[5] P. Nayeri, F. Yang, and A. Z. Elsherbeni, *Reflectarray Antennas: Theory, Designs, and Applications*. Hoboken, NJ, USA: Wiley, 2018.

[6] S. V. Hum and J. Perruisseau-Carrier, "Reconfigurable Reflectarrays and Array Lenses for Dynamic Antenna Beam Control: A Review," *IEEE Trans. Antennas Propag.*, vol. 62, no. 1, pp. 183-198, Jan. 2014.

[7] H. Yang, et al. "A 1-bit 10 x 10 reconfigurable reflectarray antenna: design, optimization, and experiment." *IEEE Trans. Antennas Propag.*, vol. 64, no. 6, pp. 2246-2254, Jun. 2016.

[8] R. Deng, F. Yang, S. Xu, and M. Li, "A 100-GHz metal-only reflectarray or high-gain antenna applications," *IEEE Antennas Wireless Propag. Lett.*, vol. 15, pp. 178-181, 2016.

[9] J. Huang, "Bandwidth study of microstrip reflectarray and a novel phased reflectarray concept", *Proc. IEEE Int. Symp. Antennas Propag.*, pp. 582-585, 1995.

[10] E. Carrasco, Jose A. Encinar, and Mariano Barba. "Bandwidth improvement in large reflectarrays by using true-time delay." *IEEE Trans. Antennas Propag.*, vol. 56, no. 8, pp. 2496-2503, 2008.

[11] D. M. Pozar, "Bandwidth of reflectarrays", *Electron. Lett.*, vol. 39, no. 21, pp. 1490-1491, Oct. 2003.

[12] Y. Mao, et al. "A novel phase synthesis approach for wideband reflectarray design." *IEEE Trans. Antennas Propag.*, vol. 63, no. 9, pp. 4189-4193, 2015.

[13] J. Yin, Q. Lou, H. Wang, Z. N. Chen and W. Hong, "Broadband Dual-Polarized Single-Layer Reflectarray Antenna with Independently Controllable 1-Bit Dual Beams," *IEEE Trans. Antennas Propag.*, vol. 69, no. 6, pp. 3294-3302, June 2021.

[14] H. Luyen, Z. Zhang, J. H. Booske and N. Behdad, "Wideband beam-steerable reflectarrays based on minimum-switch topology polarization-rotating unit cells", *IEEE Access*, vol. 7, pp. 36568-36578, 2019.

[15] F. Wu, J. Wang, Y. Zhang, W. Hong and K. -M. Luk, "A Broadband Circularly Polarized Reflectarray with Magneto-Electric Dipole Elements," *IEEE Trans. Antennas Propag.*, vol. 69, no. 10, pp. 7005-7010, Oct. 2021.

[16] K.-M. Luk, and H. Wong. "A new wideband unidirectional antenna element." *Int. J. Microw. Opt. Technol.*, vol. 1, no. 1, pp. 35-44, Jun. 2006.

[17] K. Luk and B. Wu, "The Magnetolectric Dipole—A Wideband Antenna for Base Stations in Mobile Communications," *Proceedings of the IEEE*, vol. 100, no. 7, pp. 2297-2307, July 2012.

[18] K. B. Ng, H. Wong, K. K. So, C. H. Chan and K. M. Luk, "60 GHz Plated Through Hole Printed Magneto-Electric Dipole Antenna," *IEEE Trans. Antennas Propag.*, vol. 60, no. 7, pp. 3129-3136, July 2012.

[19] S. Liu, H. Sato and Q. Chen, "A Wideband, 1 bit Transmitarray Antenna Design With Flat Gain Response," *IEEE Transactions on Antennas and Propagation*, vol. 68, no. 10, pp. 7046-7055, Oct. 2020.

[20] Y. Rahmat-Samii, "Reflector Antennas," in *Antenna Handbook*, Van Nostrand Reinhold Company, Inc., pp. 15-61, 1988.

[21] M. Wang, S. Xu, F. Yang and M. Li, "A 1-bit bidirectional reconfigurable transmit-reflect-array using a single-layer slot element with PIN diodes", *IEEE Trans. Antennas Propag.*, vol. 67, no. 9, pp. 6205-6210, Sep. 2019.

[22] B. Xi, Y. Xiao, K. Zhu, Y. Liu, H. Sun and Z. Chen, "1-Bit Wideband Reconfigurable Reflectarray Design in Ku-Band," *IEEE Access*, vol. 10, pp. 4340-4348, 2022.

[23] J. Han, et al. "A wideband 1-bit 12x 12 reconfigurable beam-scanning reflectarray: design, fabrication, and measurement." *IEEE Antennas Wireless Propag. Lett.*, vol. 18, no. 6, pp. 1268-1272, Jun. 2019.

[24] H. Luyen, J. H. Booske and N. Behdad, "2-Bit Phase Quantization Using Mixed Polarization-Rotation/Non-Polarization-Rotation Reflection Modes for Beam-Steerable Reflectarrays," *IEEE Trans. Antennas Propag.*, vol. 68, no. 12, pp. 7937-7946, Dec. 2020.

[25] F. Wu, J. Wang, et al. "Wideband and low cross-polarization transmitarray using 1 bit magnetolectric dipole elements," *IEEE Trans. Antennas Propag.*, vol. 69, no. 5, pp. 2605-2614, May 2021.